Structural Engineering and Mechanics, Vol. 12, No. 6 (2001) 595-614
DOI: http://dx.doi.org/10.12989/sem.2001.12.6.595

Analytical and experimental postbuckling of conditioned cables*

L. Rivierre†

France Télécom, CNET Lannion-DTD/IBL, BP40, 22307 Lannion cedex, France

O. Polit‡

LMpX-Université Paris X-1 Chemin, Desvallières-92410 Ville d'Avray, France

J.L. Billoët‡

LM²S-UPRES A8007-ENSAM, 151 Bd de l'Hopital-75013 Paris, France

Abstract. This paper studies the behaviour of a homogeneous cable in a horizontal rigid duct and loaded by an axial compressive force. This behaviour is characterized by spatial buckling modes, named sinusoidal and helical, due to friction and total or partial cable locking. The evaluation of critical buckling loads involved by drilling technology has been studied by many authors. This work presents a new formulation, taking the friction effects into account, for the transmission of the axial load during the postbuckling process. New analytical expressions of pitches in both buckling cases are also given. A life-sized bench is presented, which permits to study the laying of optical fiber cables by squeezing them into an underground duct. Finally, analytical solutions are compared with experimental tests and finite element simulations.

Key words: beam; buckling; postbuckling; boundary conditions; contact analytical; experimental; finite element results.

1. Introduction

This paper deals with the problem of a homogeneous cable loaded by an axial compressive load into a horizontal cylindrical rigid duct with an end stop. An axial compression load is applied to the cable and buckling instabilities can be generated by friction accumulation and total or partial cable head locking. The lateral displacement of the cable is conditioned by a rigid duct which has a direct influence on the buckling mode. Two global spatial instabilities called sinusoidal and helical buckling can appear. The aim of this paper is to give new analytical expressions for the sinusoidal and helical pitches and the transmission of the axial load during the postbuckling state. Then, a validation of the formulation is presented using experimental and numerical approaches.

The process of buckling and post-buckling during an increasing compressive load is described in

† Ph.D. Student
‡ Professor

*The earlier version of this paper appears in proceedings of ASEM'99, 23-25 August 1999, Seoul, Korea

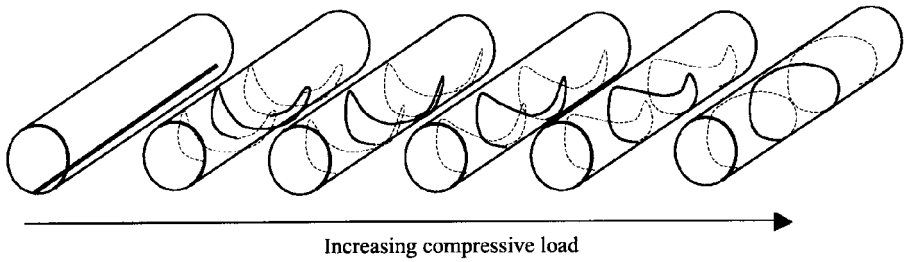

Fig. 1 Sinus and helical configurations of a cable in a duct

Fig. 1. As long as the load is less than a first critical load F_{sin}, the cable is straight in the lower part of the duct. From this value, the cable buckles in a sinusoidal configuration and snakes in the lower part. Sinus half-waves increase until a second critical load F_{hel} is reached. Then the cable buckles into a helical shape by a snap-through process. Such buckling phenomena were first studied in (Lubinski *et al.* 1962) for the helical buckling mode. Bogy and Paslay (1964) paper deals with the sinusoidal buckling mode and their work was followed up by Dawson and Paslay (1984). In these works, a relation between force and helix pitch is given by Lubinski and in the case of the sinusoidal configuration, critical buckling load and pitches are given by Bogy. The transmission of the axial load was studied in Wu (1992) but contact force is overestimated as it will be shown in this paper.

Three different parts can be defined in the following:

The first one concerns the analytical developments for the two buckling cases. An energetic approach (Cheatham and Patillo 1984, Chen *et al.* 1990, Wu and Juvkam-Wold 1993) gives the two critical loads named sinusoidal and helical and new relations between pitches and axial loads are deduced. A geometrical perturbation without energy is applied to a straight cable and the potential energy variation is studied. Then, new analytical expressions for the axial load in the post-buckling configuration are presented, taking the real participation of the weight in the contact force into account. A comparison with previous works is given.

In the second part, a presentation of a life-sized experimental bench is given.

Suryanarayana and McCann (1994) showed that, in the case of a short bench, the critical load is the minimal value obtained by the two integer values of n which frame the real solution. Large differences can be observed between these two limit values and the experimental buckling load is different from that on a long bench test. Therefore, a long bench test has been chosen and some tests have been conducted on a straight duct 35 meter long. For both axial transmission load and variable pitches, experimental results are compared to analytical expressions.

Finally, in the last part, finite element simulations are presented in order to estimate buckling loads and pitches. The friction influence is also evaluated and some comparisons with analytical relations and experimental values are given.

All the given comparisons with experimental and numerical simulations verify the accuracy of our analytical approach for both buckling and post-buckling configurations.

2. Analytical approach

This section concerns the two cable configurations and gives analytical expressions for the two

critical buckling loads and the sinusoidal and helical pitches. Lubinski pitch-load relations are classically used but those relations are only valid at the snap-through moment from sinusoidal to helical configuration. They do not apply afterwards. Therefore, new analytical values are presented for sinus and helix pitches as functions of the axial load. The last section is dedicated to the transmission of the axial load during the buckling configuration.

In the worst case, helical buckling can generate so large a frictional drag that an increasing axial load does not permit the introduction of the cable inside the duct any longer. The contact force generated by the cable on the duct is a function of the cable configuration. In the sinus case, the contact force is estimated in Wu and Juvkam-Wold (1995) while for the helical configuration, two different values are given in Mitchell (1986) and Sadiq and Juvkam-Wold (1995). It can be noted that Sadiq is the only one that has provided an experimental bench to validate his analytical value. In the present work, Sadiq contact force is used in our analytical developments.

2.1 Critical pitches and loads

This section is dedicated to the analytical study of the critical buckling loads and pitches for the sinusoidal and helical buckling modes. Then the pitch is expressed as a function of the axial compressive load applied to the cable.

An energetic method is used to determine the critical loads. Several hypotheses must be considered: the system is frictionless, the cable has a homogeneous bending stiffness and is always in contact with a rigid long duct which is perfectly circular, and the duct is supposed to be long. This last hypothesis is often forgotten but Suryanarayana and McCann (1994) show that a short length has a direct influence on critical pitches and loads. An angular perturbation $\alpha(x)$ (see Fig. 2), without energy contribution, similar to the buckling mode, is applied to the initial straight cable. Under this perturbation, a new equilibrium state must be determined. Therefore, the first order variation of the potential energy (1) must be equal to zero and this new equilibrium is stable if the second order variation of the potential energy (2) is positive. The stability of each buckling configuration has been demonstrated in Chen (1988) using the second variation of the potential energy.

$$\Delta V = \Delta U + \Delta W_{\text{ext}} = 0 \tag{1}$$

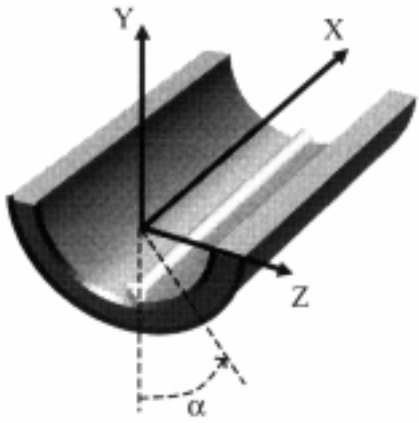

Fig. 2 Coordinate system and angular perturbation

$$\frac{1}{2}\Delta^2 V = \frac{1}{2}\Delta^2 U + \frac{1}{2}\Delta^2 W_{\text{ext}} + \Delta U \Delta W_{\text{ext}} \tag{2}$$

where the work of the external load ΔW_{ext} is the work of the applied compressive load ΔW_F and the work of the weight ΔW_{weight}. The bending energy is denoted ΔU.

Sinusoidal buckling

In the case of the sinusoidal buckling mode, the perturbation, see Fig. 2, is given by:

$$\alpha(x) = \alpha_0 \sin\left(\frac{n\pi x}{L}\right) \tag{3}$$

and we have:

$$\begin{aligned} \Delta U &= -\frac{r^2 EI}{4} L \alpha_0^2 \left(\frac{n\pi}{L}\right)^4 \\ \Delta W_{\text{weight}} &= -\frac{w_e r L}{4} \alpha_0^2 \\ \Delta W_{F_s} &= \frac{F_s L}{4}\left(r\alpha_0 \frac{n\pi}{L}\right)^2 \end{aligned} \tag{4}$$

where F_s stands for the axial load associated to the sinus configuration.

Therefore, ΔV is deduced from (1) using (4). Then, the critical buckling load is obtained and stated as:

$$F_s = EI\left(\frac{n\pi}{L}\right)^2 + \frac{w_e}{r}\left(\frac{L}{n\pi}\right)^2 \tag{5}$$

It must be denoted that when r tends toward infinity, meaning that the duct is far from the beam, Eq. (5) gives Euler's critical load.

Furthermore, without friction and for a long bench, a constant half-sinus length denoted $P_s = \frac{L}{n}$ can be defined and Eq. (5) takes the following form:

$$F_s = EI\left(\frac{\pi}{P_s}\right)^2 + \frac{w_e}{r}\left(\frac{P_s}{\pi}\right)^2 \tag{6}$$

Fig. 3 gives the graphic representation of Eq. (6), for given values for EI, w_e, r, and shows the existence of a minimum value which is the minimal critical buckling load F_{sin}, associated with a specific pitch denoted P_{sin}. Therefore, based on Eq. (6), a minimisation of F_s with respect to P_s is carried out and the sinus pitch is given by:

$$P_{\text{sin}} = \sqrt[4]{\frac{EI\pi^4 r}{w_e}} \tag{7}$$

Introducing (7) into (6), the sinus critical buckling load is deduced as:

$$F_{\text{sin}} = 2\sqrt{\frac{EIw_e}{r}} \tag{8}$$

Helical buckling

For the helical buckling case, the same method is used in order to find P_{hel} and F_{hel}. The angular

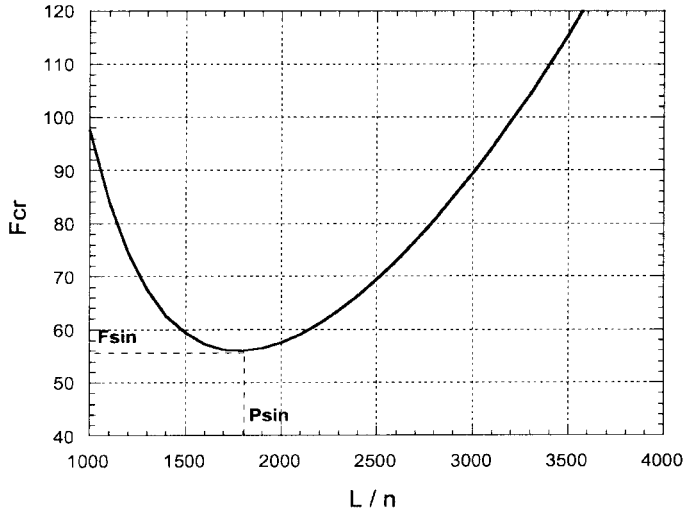

Fig. 3 The sinus buckling load curve

perturbation is defined as:

$$\alpha(x)=\frac{2\pi nx}{L} \tag{9}$$

From Lubinski *et al.* (1962), the bending energy U and the work of the external loads have the following forms:

$$\Delta U = -8EILr^2\left(\frac{n\pi}{L}\right)^4$$

$$\Delta W_{\text{weight}} = -w_e L r$$

$$\Delta W_{F_h}=2F_h L\left(\frac{n\pi r}{L}\right)^2 \tag{10}$$

Therefore, using Eq. (1), the relation between critical buckling load and pitch is retrieved and we have:

$$F_h=EI\left(\frac{2n\pi}{L}\right)^2+\frac{w_e}{2r}\left(\frac{L}{n\pi}\right)^2 \tag{11}$$

Finally, the helical critical pitch and load are deduced using the above methodology:

$$P_{\text{hel}} = 2^{3/4}\sqrt[4]{\frac{EI\pi^4 r}{w_e}},\quad F_{\text{hel}}=2\sqrt{2}\sqrt{\frac{EIw_e}{r}} \tag{12}$$

From those expressions, the helical pitch and the helical critical load are very close to sinus values, see Eqs. (7) and (8). Ratios of $2^{3/4}$ and $\sqrt{2}$ can respectively be noticed.

Critical pitches and loads presented in this section are obtained neglecting the friction effect. It must be noticed that friction is always present and pitches of the sinusoid and the helix are not constant along the cable.

2.2 Post-buckling force-pitch relation

In order to express a variable pitch as a function of the cable weight and the axial load, Eqs. (6) and (11) must be used. Only one half-sinus and one helix are studied and $P = L/n$ is introduced in these equations. We have for the sinusoidal case:

$$\frac{w_e}{r}P_s^4 - \pi^2 F_s P^2 + EI\pi^4 = 0 \tag{13}$$

and in the helical case, we obtain:

$$\frac{w_e}{r}P_h^4 - 2\pi^2 F_h P^2 + 8EI\pi^4 = 0 \tag{14}$$

Four solutions can be found for P. Therefore, following constraints must be taken into account:

$$\begin{aligned} &P_s(F_{\sin})P_{\sin} \quad \text{and} \quad \lim_{w_e \to 0} P_s = \pi\sqrt{\frac{EI}{F_s}} \quad \text{Sinusoidal case} \\ &P_h(F_{\text{hel}})P_{\text{hel}} \quad \text{and} \quad \lim_{w_e \to 0} P_h = 2\pi\sqrt{\frac{EI}{F_h}} \quad \text{Helical case} \end{aligned} \tag{15}$$

Solutions obtained for a weightless cable are deduced from the resolution of Eqs. (13) and (14) with w_e equal to zero. Finally, for each configuration and for a given load F_s or F_h associated to a fixed position in the duct, variable pitches are given by (Rivierre *et al.* 1999):

$$P_s = \pi\sqrt{\frac{rF_s}{2w_e}\left(1 - \left(1 - \frac{F_{\sin}^2}{F_s^2}\right)^{1/2}\right)} \quad \text{for} \quad F_s \in [F_{\sin}, F_{\text{hel}}[\tag{16}$$

$$P_h = \pi\sqrt{\frac{rF_h}{w_e}\left(1 - \left(1 - \frac{F_{\text{hel}}^2}{F_h^2}\right)^{1/2}\right)} \quad \text{for} \quad F_h \geq F_{\text{hel}} \tag{17}$$

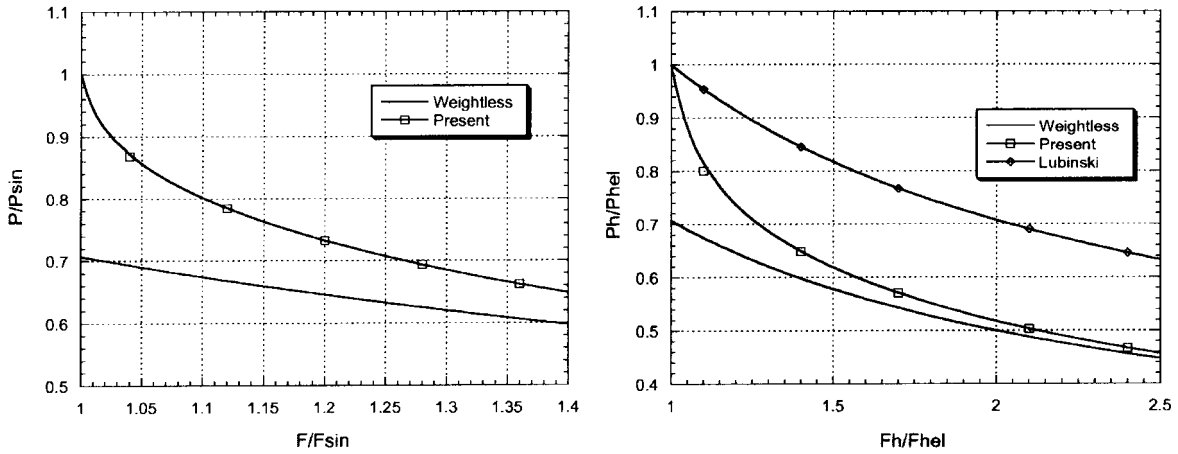

Fig. 4 Analytical comparisons of pitch values with respect to the axial load

The present Eq. (17) can be compared with the classical equation used in the litterature relating force and pitch (Lubinski *et al.* 1962) in order to estimate the variable pitches:

$$P = 2\pi\sqrt{\frac{2EI}{F}} \tag{18}$$

It must be noticed that Eq. (18) can be only used when the cable buckles in the helical configuration and are not valid during the post-buckling process. Furthermore, this equation is different by a factor $\sqrt{2}$ from our relation given in Eq. (15) which is also given by Cheatham and Patillo (1984), Miska and Cunha (1995). Fig. 4 presents pitch and load values obtained using Eq. (18) and our Eq. (17). In Fig. 4, one can observe that our pitch is always contained within Lubinski values and the weightless case values. Results obtained with our expression are more realistic because the external force work gives two terms: the work of the compressive load which increases and the work of the weight which is constant. The more the load increases, the less important the weight effect is; therefore the value must converge to the weightless solution as it is observed in Fig. 4.

At this stage, friction cannot be taken into account and will be the subject of the next section.

2.3 Transmission of the axial load

The knowledge of the critical load permits to estimate the transmission of the axial load during the postbuckling process. For a given axial compressive load *F*, three different configurations must be studied: the first one being the straight or unbuckled one ($F \le F_{\sin}$), the second the sinusoidal one ($F_{\sin} < F \le F_{\text{hel}}$) and the last one the helical configuration ($F > F_{\text{hel}}$), see Fig. 1. In order to take friction effect into account, Coulomb's classical law is used, see Eq. (19), as in Wu and Juvkam-Wold (1993), Wu (1995).

$$\| t_t \| \le \mu \| t_n \| \quad \text{and} \quad \begin{array}{ll} \| t_t \| < \mu \| t_n \| \Rightarrow \upsilon_t = 0 & \text{no sliding} \\ \| t_t \| = \mu \| t_n \| \Rightarrow \upsilon_t \| > 0 & \text{sliding} \end{array} \tag{19}$$

In this case, a relation between the tangential t_t and the normal term t_n of the contact forces (see Fig. 5) is expressed and gives the tangential sliding υ_t. If the tangential force reaches $\mu \| t_n \|$ value, then the body slides. When a massive structure is in contact with a rigid surface, the differential equation given below has to be solved in order to obtain the axial load moving value:

$$\frac{dF(x)}{dx} = \mu N(x) \tag{20}$$

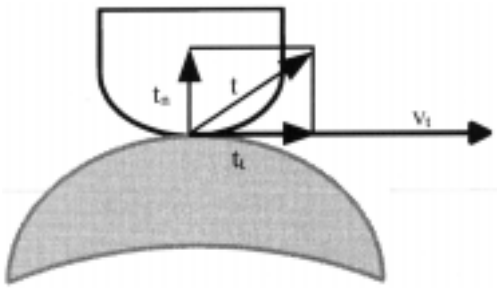

Fig. 5 The friction between two bodies

In the case of a pressure load, an integration with respect to the contact length must be made. Thus, integration of Eq. (20) is carried out with respect to the contact length. For a cable in a circular duct, a general differential equation of the axial load transmission is given by:

$$\frac{dF(x)}{dx} = \mu(N_1(x) + \lambda N_2)$$
$$= \mu\left(\delta_i \beta(\alpha(x)) w_e + \lambda \frac{rF^2}{\eta EI}\right) \tag{21}$$

in which the normal force is split up in two terms: the first one N_1 is the weight participation and the second one λN_2 takes the cable configuration into account (straight, sinus or helix). For an unbuckled cable, $\lambda = 0$ whereas $\lambda = 1$ for sinusoidal and helical configurations.

For the unbuckled case, linear weight only takes place in the frictional drag analysis. The resolution of this differential equation gives the well known relation:

$$F(x) = F - \mu w_e x \tag{22}$$

On the other hand and in the general buckling case, wall contact force N_2 is a function of the variable η which characterizes the geometric cable configuration. For the sinusoidal buckling case, Wu (1995) identifies $\eta = 8$ even though different values of η are given for the helical one: Mitchell 1986) gives $\eta = 4$ and (Sadiq and Juvkam-Wold 1995) $\eta = 2$. In the present work, Sadiq's choice is used because his value was validated by an experimental procedure. Therefore, we have:

$$N_{2\sin} = \frac{rF^2}{8EI} \quad \text{and} \quad N_{2\text{hel}} = \frac{rF^2}{2EI} \tag{23}$$

Since N_2 is defined, the weight contribution N_1 in Eq. (21) remains to be characterized. In Wu and Juvkam-Wold (1993) and for both sinus and helical cases, authors choose $\delta i \beta(\alpha(x))=1$. As it will be discussed later during the numerical comparisons, Wu overestimates the weight participation in Eq. (21) because $N_1 = w_e$ is always assumed. In fact, the cable is not straight anymore on the lower part of the duct and the value cannot be 1 because only the projection part in the normal direction to the surface must be considered. It can be noticed that the pressure distribution generated by the weight of the cable is not constant. During experimentation it has been noticed that, for sinusoidal buckling, the cable is always in the lower part of the duct and the amplitude of the sinus is never higher than the horizontal middle plane of the duct. This amplitude depends on the axial load F (see Appendix A). In order to simplify the integral expression for N_1, a function ϕ is introduced in Eq. (21). ϕ is expressed as a function of the axial load for each sinusoid and we assume:

$$\phi = \delta_i \beta(\alpha(x)) w_e \tag{24}$$

In the sinusoidal case, ϕ is a function of the maximal amplitude and is different for each sinusoid.

On the other hand and for the helical case, sliding is penalized when the cable is in the lower part of the duct because the weight effect is maximum, even though in the higher part, the weight effect tends to move the cable away from the duct wall and sliding is made easier. Therefore, chosen values are $\delta_i = 1$ in the lower part and $\delta_i = -1$ in the upper part of the duct. Therefore, ϕ takes a constant value for all helixes because the cable always makes a full turn around the duct.

Finally, the values of ϕ are obtained for each configuration (see appendix A for detail calculations)

and we have, for the sinusoidal case:

$$\phi = 2\frac{w_e}{\pi\bar{F}}\sin\left(\frac{\pi\bar{F}}{2}\right) \quad \text{with} \quad \bar{F} = \frac{F - F_{\sin}}{F_{\text{hel}} - F_{\sin}} \tag{25}$$

and for the helical case:

$$\phi = 0 \tag{26}$$

The transmission of the axial load for sinusoidal and helical configurations is deduced from Eq. (21) using the normal contact force previously obtained (see Appendix for detail calculations) and we have, for the sinusoidal case:

$$F_s(x) = 2\bar{\phi}F_{\sin}\tan\left(\arctan\left(\frac{F}{2\bar{\phi}F_{\sin}}\right) - \mu x\frac{w_e\bar{\phi}}{F_{\sin}}\right) \quad \text{with}\,\bar{\phi} = \sqrt{\frac{\phi}{2w_e}} = \sqrt{\frac{\sin\left(\frac{\pi\bar{F}}{2}\right)}{\pi\bar{F}}} \tag{27}$$

and, for the helical case:

$$F_h(x) = \left(\frac{\mu r}{2EI}x + \frac{1}{F}\right)^{-1} \tag{28}$$

Eqs. (27) and (28) are different from the ones given in Wu and Juvkam-Wold (1995).

It must be noticed that sinusoidal buckling appears when the load values are included within $F_{\sin}$ and F_{hel}. But as it is shown in Eq. (16), the half sinusoid pitch is a function of the axial load F_s at the starting point of the sinus. Therefore, the buckling length for the sinusoidal case cannot be directly expressed.

For the helical case, the transmission of the axial load only depends on the position in the duct, given by the coordinate x. The buckling length, as a function of the axial load F, is deduced from Eq. (28) for a given F with $F_{\text{hel}} = F_h(L_{\text{hel}})$ and we have:

$$L_{\text{hel}} = \frac{2EI}{\mu r}\left(\frac{1}{F_{\text{hel}}} - \frac{1}{F}\right) \tag{29}$$

The buckling length used in Wu and Juvkam-Wold (1995) is different and takes the following expression:

$$L_{\text{hel}} = \frac{F_{\sin}}{\mu w_e}\left(\arctan\left(\frac{F}{\sqrt{2}F_{\sin}}\right) - \arctan\left(\frac{F'_{\text{hel}}}{F_{\sin}}\right)\right) \tag{30}$$

where F'_{hel} denotes the helical buckling load and is given by:

$$F'_{\text{hel}} = 2(\sqrt{2} - 1)\sqrt{\frac{EIw_e}{r}} \tag{31}$$

This last equation can be compared with our helical buckling load, defined by Eq. (12), which is called “average helical buckling” load in Wu and Juvkam-Wold (1995).

The evaluation of all these analytical expressions are given in the next section by comparison with experimental results.

3. Experimental drag analysis

In this section, experimental drag analysis is presented in order to compare analytical results with measurements. Some authors (Dillinger *et al*. 1983, Lubinski 1987) use experimental benches to derive empirical solutions and find a critical buckling load very close to our analytical expression given in Eq. (12). But all those benches are small: 3.65 meters in Suryanarayana and McCann (1994), 3 meters in Wu (1992), Wu and Juvkam-Wold (1993). Only Salies *et al*. (1994, 1995) use a relatively long bench, 10 and 24 meters long, but his helical critical buckling load is equal to our sinusoidal critical load.

Therefore, a long bench test is chosen in this work and some tests are carried out on a 35 meter straight duct. This length also permits to analyse experimental variable pitches with respect to the analytical solutions expressed in the first part of this paper without boundary condition influences and short length effects.

3.1 Presentation of the experimental bench

The bench test used at France Télécom R&D Lannion (Boulharts-Campion 1998) is presented in Fig. 6. This bench allows to estimate the postbuckling configurations of the cable and also the frictional drag. For these purposes, translucent ducts with variable lengths (5 to 45 meters) permit to measure pitch lengths using a measuring metric system located along the duct. Furthermore, this bench test is a dynamic bench test because the cable is not fixed at both extremities and measurements are made with a moving cable. Therefore, the axial load can be collected at different points on the 45 meter long straight duct, and compared with analytical solutions for different pushing loads. The difference with an oil-rig bench test is that the aim is to estimate the load applied by the bit onto the ground and not the value of the load necessary to introduce a cable in a duct.

3.2 Transmission of the axial load

First, a sensitivity analysis is carried out for different lenghts of duct: 15, 25 and 35 meters, with the same duct diameter of 0.042 meters and the same length of 15 meters with different duct diameters: 0.028, 0.042 and 0.069 meters. The characteristics of the cable are:

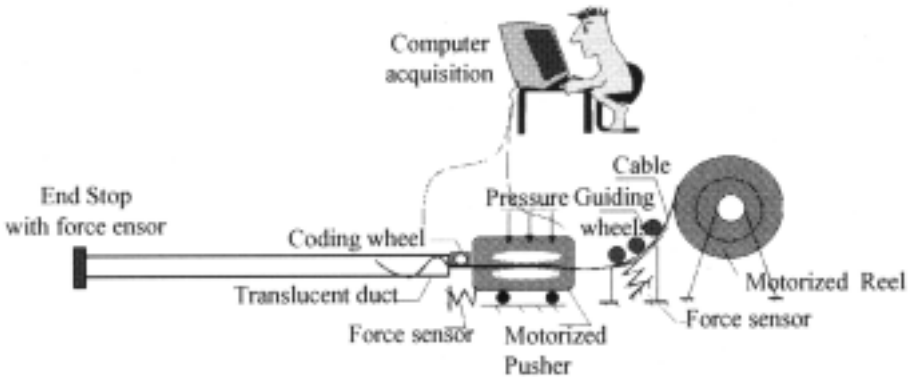

Fig. 6 The experimental bench test

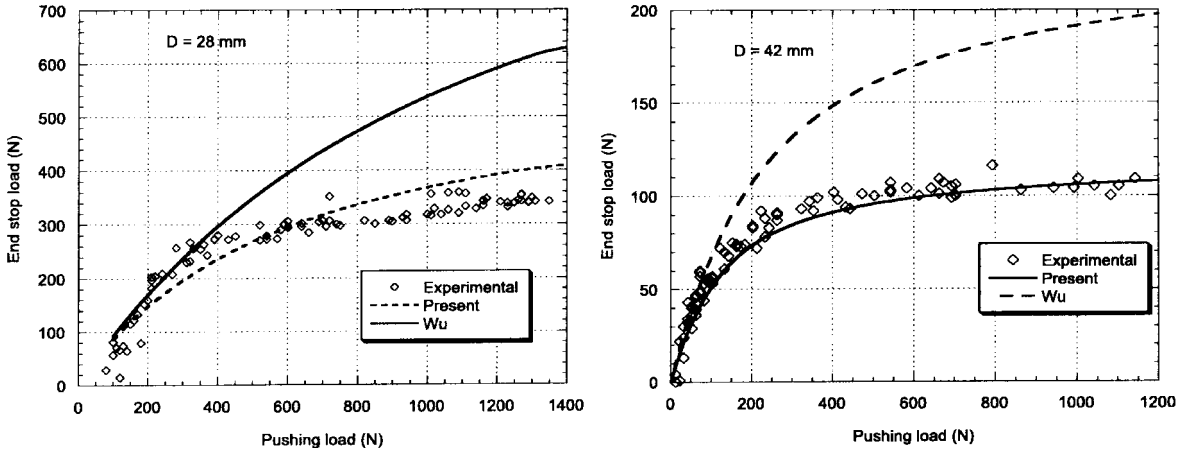

Fig. 7 Experimental results: Load curves for different duct diameters and a length of 15 meters

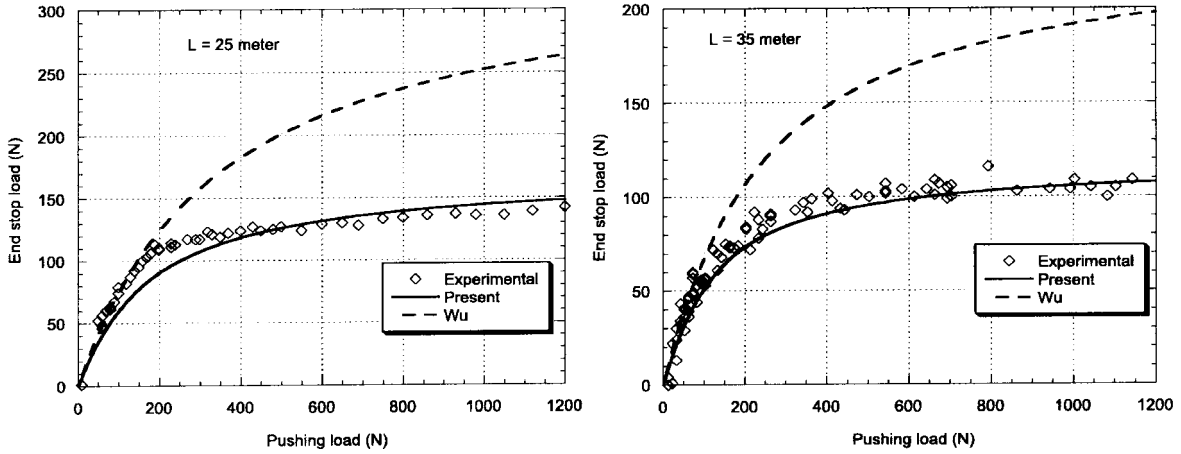

Fig. 8 Experimental results: Load curves for different duct lengths and a diameter of 0.042 meters

$$w_e = 12 \times 10^{-4} \text{ N/mm}, \quad r = 13.75 \text{ mm}, \quad L = 35 \text{ m} \quad EI = 8.99 \times 10^6 \text{ N} \cdot \text{mm}^2.$$

The friction coefficient is taken equal to 0.3, measurement achieved using another experimental bench test developed at France Télécom R&D Lannion (Mignon *et al*. 1998).

Figs. 7 and 8 give the end stop load value with respect to the pushing load value for different duct lengths and diameters. These experimental results permit to evaluate the influence of the two main geometrical parameters on the behaviour of the cable. Experimental results obtained are in great accordance with our analytical model. Furthermore, values deduced from Wu model always overestimate the end stop loads. In the case of the larger diameter (0.069 meter), a gap between analytical and experimental values is observed and may be due to the duct ovalization which has been observed. This phenomenon generates a greater contact force.

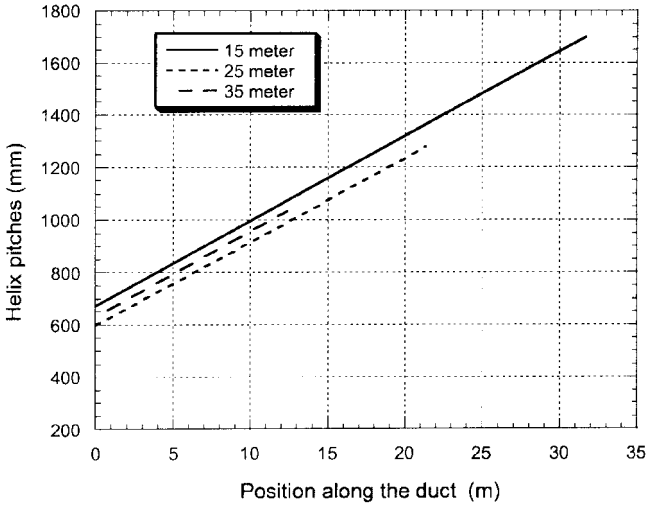

Fig. 9 Experimental results: Helical pitcal pitch linearisation for different duct lengths

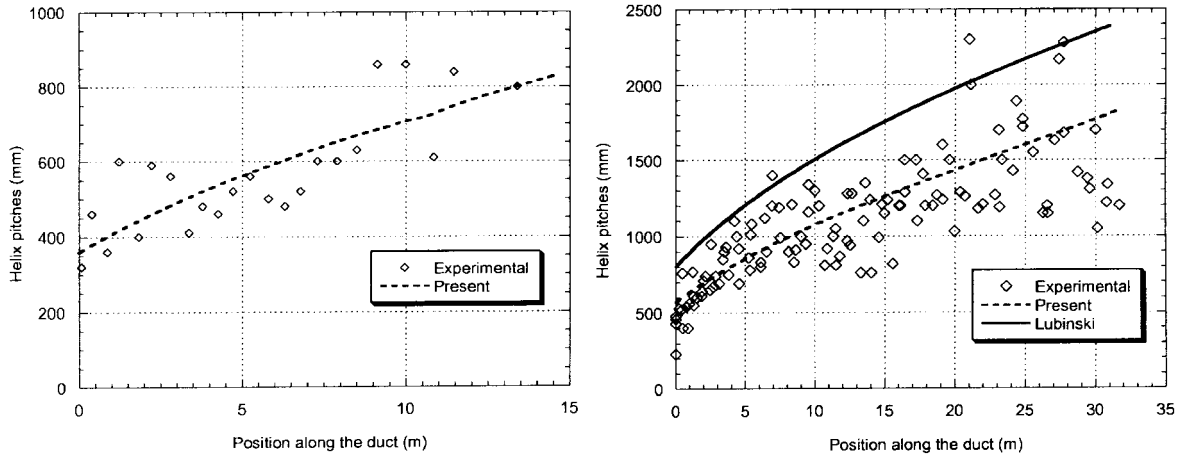

Fig. 10 Experimental results: Helical pitch values for two geometrical duct configurations

3.3 The variable pitches

As previously indicated and using a metric system, this bench allows to measure helix pitches. Fig. 9 presents the linearization of the values obtained from five experimental tests for each length (15, 25 and 35 meters) and for the 0.042 meter duct diameter. The same slope is obtained and the pitch increases from the start to the end of the duct: this is due to accumulated friction.

Furthermore, Fig. 10 gives a comparison for two geometrical duct configurations (length, diameter) between experimental and analytical helix pitch length using Eqs. (17) and (27). Lengths of 15 and 35 meters with respectively duct diameters of 0.028 and 0.042 meters are considered. For both cases, analytical values are very close to experimental measurements. It must be noticed that the variation of the experimental pitch length comes from local friction problems and geometrical

imperfections of the cables because the cable was previously rolled up on a big wheel.

4. Finite element analysis

In the litterature, few examples of finite element simulations are available to evaluate buckling and post-buckling of conditioned cables. Finite element simulations must take the 3D buckling process into account in this study. 3D beam elements (B31) for the cable and contact elements (ITT31) for the rigid duct, from ABAQUS (Hibbitt *et al.* 1999) finite element software, are used. The boundary conditions are a fixed hinge at the stop and a hinge with an axial displacement at the duct entrance cable node. Simulations use the implicit version of ABAQUS, taking geometrical non-linearities into account and the resolution uses line search control for the incrementation.

In order to generate buckling and post-buckling phenomena, a small geometrical imperfection is introduced to initiate axial and bending coupling. A half-sinusoidal wave of one meter (the total length is 35 meters) with a one degree angle is introduced. For all the finite element simulations, datas are the same as for the experimental drag analysis.

With these values critical pitches and loads are obtained using analytical expressions given in the previous section. We have:

$$F_{\text{sin}} = 56\ N, \quad F_{\text{hel}} = 79.2\ N, \quad P_{\text{sin}} = 1780\ \text{mm}, \quad P_{\text{hel}} = 2993\ \text{mm}.$$

4.1 Buckling with force control

In order to estimate the critical sinusoidal buckling load, first simulations are based on a force control in order to introduce the cable in the rigid duct.

Fig. 11 presents the finite element model with 2040 elements, 3402 nodes and 8172 degrees of freedom. Load incrementations are small enough in order to prevent a jump on a wrong postbuckling path.

Numerical values obtained when $F_{\text{num}}/F_{\text{sin}} = 1$, see Fig. 11, are $F_{\text{sin}} = 55.44$ N and $P_{\text{sin}} = 1700$ m.

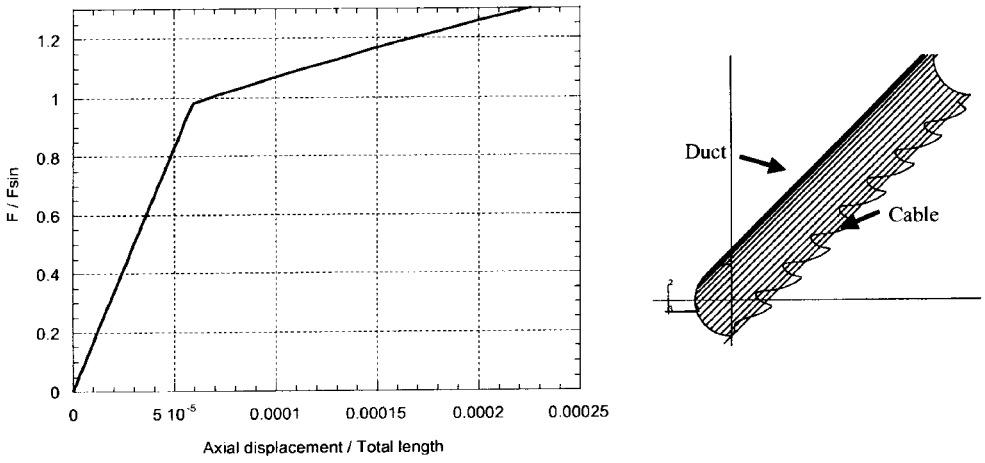

Fig. 11 Finite element simulations: Load control case and the sinus configuration

Table 1 Half sinus pitches with respect to the length and the duct diameter

R_{duct} (mm)	500	500	500	500	100	100	100	20	20
L_{duct} (m)	10	20	30	45	10	20	30	10	20
F_{sin} (N)	9	9	9	9	20	20	20	46	46
F_{load} (N)	10	10	10	10	23	23	23	51	51
$P_{analytical}$ (mm)	4303	4303	4303	4304	2877	2877	2877	1924	1924
$P_{numerical}$ (mm)	4584	4130	4294	4337	2949	2948	2948	1949	1949
error (%)	6.1	−4	−0.2	0.8	2.5	2.47	2.47	1.3	1.3

With respect to the analytical reference given above, these numerical values deviate by less than 5%.

Other simulations are conducted with different values for the length and the diameter of the duct. The half sinus pitches length results are presented in Table 1. A very good agreement is found in Table 1 between numerical values and the analytical ones. The error is always less then 6%.

A force control approach does not permit to observe the helical buckling because the compressive load decreases during the snap-through process. Therefore, a displacement control is used to reach the helical buckling mode.

4.2 Buckling with displacement control

The finite element model is the same than the one used in 4.1, however the beam length L is reduced to 15 m, because a lot of instabilities appears due to the snap through phenomenon and the contact conditions.

An exemple of the helical configuration obtained numerically is given in Fig. 12 while the load evolution with respect to the displacement is presented in Fig. 13. In Fig. 13, the sinusoidal mode and the helical mode appearances are visible and the snap through with a rigidity loss just before

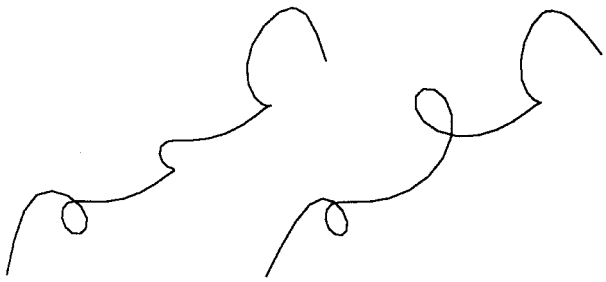

Fig. 12 Finite element simulation: Helical configuration cable

Table 2 Comparisons between analytical and numerical critical load values and pitches

	F_{sin} (N)	F_{hel} (N)	P_{sin} (mm.)	P_{hel} (mm.)
Finite element results	55.44	81.76	1700	3000
Analytical values	56.00	79.20	1780	2993
error (%)	−1	3.2	−4.5	0.2

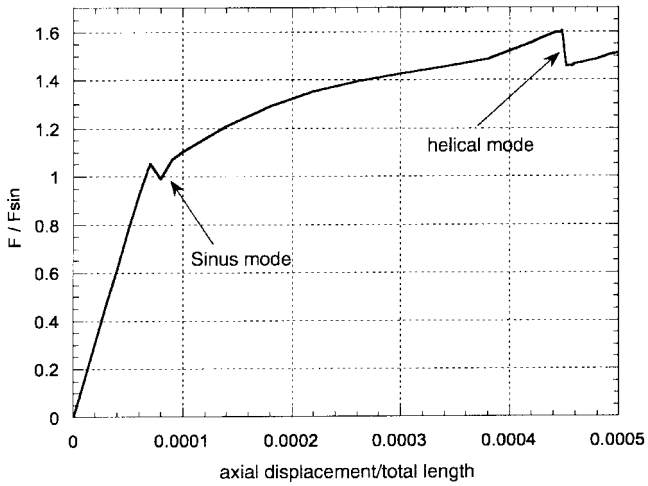

Fig. 13 Finite element simulations: Axial displacement with respect to load value

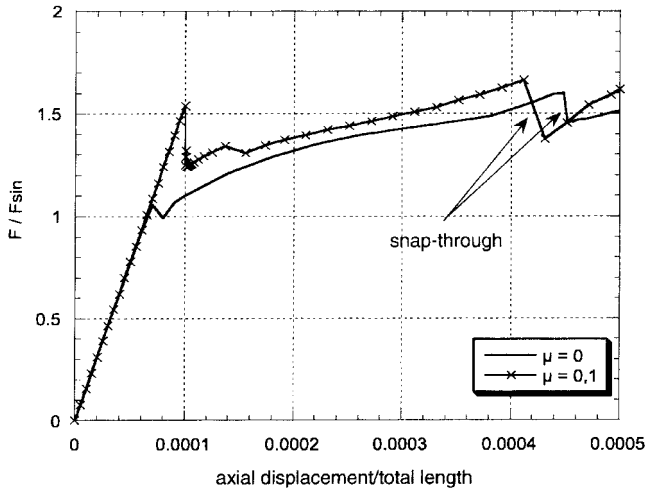

Fig. 14 Finite element simulations: Friction influence on the buckling load

the helical mode is obvious. Finally, a comparison is given between the numerical and the analytical values in Table 2 and a small difference is observed.

4.3 The friction influence

Until now and in the numerical simulations, the friction are always been neglected while it is classically included between 0.1 and 0.3. The object of this section is to evaluate the influence of the friction on the two critical load values.

The friction is opposed to the sinusoidal mode lay up as it can be seen in Fig. 14 and the critical sinusoidal buckling load increases with the friction coefficient value. It must be noticed that no result are obtained with $\mu = 0.3$ because the numerical convergence of the model becomes more difficult with the increase of the friction coefficient.

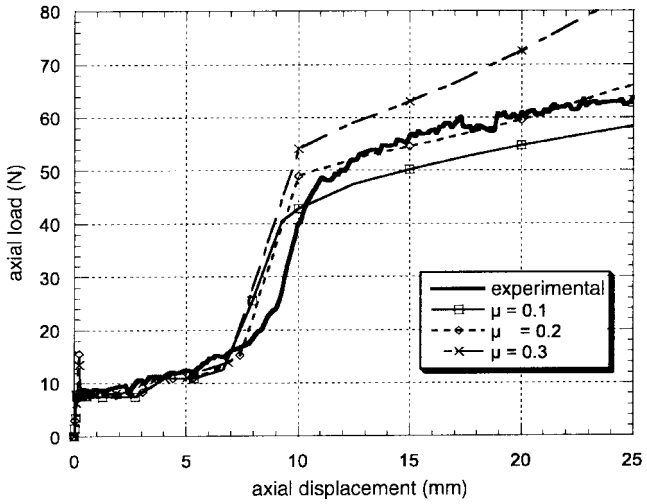

Fig. 15 Comparison between experimental and numerical results; Friction coefficient influence

On the other hand, The friction has a very small influence on the helical critical load value, see Fig. 14, because the beam leaves the duct in order to reach the upper part of the duct during the transition from the sinusoidal mode to the helical mode.

4.4 Numerical and experimental comparisons

A comparison between those numerical results and experimental tests on the life size bench is not possible because only long beam is available on this bench. In our work, a small laboratory bench has been developped (see Rivierre 2000), at the L.M.2.S of the E.N.S.A.M Paris. One of the first result is presented in Fig. 15 and shows a very good agreement between numerical and experimental results.

Furthermore, the friction influence is obvious in this figure and the experimental curve is enclosed by the numerical results.

5. Concluding remarks

In this paper, new analytical expressions have been given for critical loads and pitches in the case of sinusoidal and helical states. Furthermore, axial load transmission and analytical variable pitches are obtained, taking the weight effect into account, and allow for a new approach for the postbuckling configurations.

In order to validate this new analytical approach, several experiments have been carried out on a long bench and a very good agreement is observed between experimental measures and analytical values. The use of important length of duct (until 45 meters) allows to carry out comparisons without boundary condition influences.

Finally, some numerical results using finite element simulations on ABAQUS software are also presented and good values with respect to analytical and experimental results are obtained. The friction has been taken into account in the numerical simulations in order to evaluate his influence.

It must be noticed that very few numerical results are given in the literature on this difficult topic: buckling and post-buckling of beam with evolutionary contact boundary conditions. All the results obtained give encouraging perspectives for future numerical simulations.

Future works are also directed towards the adjustment of a laboratory experimental bench in order to characterize the buckling loads and pitches more precisely. This laboratory experimental bench has been designed and developed at the LM2S of the E.N.S.A.M. Paris. Furthermore, the influence on the postbuckling states of different rigid walls with different friction coefficients can be evaluated on this bench.

Acknowledgements

The authors want to acknowledge the France Télécom R&D Lannion for financial and technical supports and especially A. Pécot, P. Mignon, J.-L. Campion, J. Le Cam and G. Le Goff.

References

Bogy, D., and Paslay, P. (1964), "Buckling of drill pipe in an inclined hole", *J. Eng. for Industry*, **86**(2).

Boulharts-Campion, H. (1998), "Experimental and numerical studies of the pushing installation of composite cable in a duct", PhD thesis, E.N.S.A.M Paris (in French).

Cheatham, J., and Patillo, P. (1984), "Helical postbuckling configuration of weightless column under the action of an axial load", *Soc. of Petrol. Eng. J*., 467-472.

Chen, U., Lin, Y., and Cheatham, J. (1990), "Tubing and casing in horizontal wells", *J. Petrol. Tech.*

Chen, Y. (1988), "Post buckling behavior of a circular rod constrained within an inclined hole", Master's thesis, Rice University.

Dawson, R., and Paslay, P. (1984), "Drillpipe buckling in inclined holes", *J. Petrol. Tech.*, 1734-1738.

Dillinger, T., Gravley, W., and Walraven, J. (1983), "Preventing buckling in drill strength", US patent N 4,384,483.

Hibbitt, Karlson, and Sorensen (1999), *ABAQUS Version 5.8 : Theory Manual*.

Lubinski, A. (1987), "Developments in petroleum engineering", *Gulf Publishing Company*, **1**, 213-214.

Lubinski, A., Althouse, W., and Logan, J. (1962), "Helical buckling of tubing sealed in packers", *J. Petrol. Tech*., 655-670.

Mignon, P., Pécot, A., Campion, J., and Cam, J.L. (1998), "An impressive life size friction coefficient measurement technique", *Proc. of Euro Cable'98*.

Miska, S., and Cunha, J. (1995), "Helical buckling of long weightless strings subjected to axial and torsionnal loads", *Drilling Technology*, ASME, **65**, 75-78.

Mitchell, R. (1986), "Simple frictional analysis of helical buckling of tubing", *SPE Drilling Engineering*, 457-465.

Rivierre, L. (2000), "Beam buckling related to rigid wall and contacts: Analytical, experimental and numerical approaches", PhD thesis, E.N.S.A.M Paris, French.

Rivierre, L., Billoët, J.-L., and Polit, O. (1999), "Effect of conditioning boundaries on the postbuckling behavior", *Proc. of the ASEM'99*, **1**, 493-498.

Sadiq, T. and Juvkam-Wold, H. (1995), "Lateral contact force in horizontal wells: An experimental study", *Spring Drilling Conference*.

Salies, J., Azar, J., and Jr., J.S. (1994), "Experimental and mathematical modelling of helical buckling in directionnal wellbores", *presented at the Petrol. Conf. & Exhibition of Mexico*, 79-89.

Salies, J., Azar, J., and Jr., J.S. (1995), "Experimental and mathematical modeling of helical buckling of pipes in horizontal wellbores", *Drilling Technology*, ASME, **65**, 79-89.

Suryanarayana, P., and McCann, R. (1994), "Experimental study of buckling and post-buckling of literally

constrained rods: Part 1 - frictionnal sffects", *Energy-Sources Technology Conference & Exhibition*, 1-12.
Wu, J. (1992), "Buckling behavior of pipes in directional and horizontal wells", PhD thesis, Texas A&M.
Wu, J. (1995), "Slack-off load transmission in horizontal and inclined wells", *Production Operation Symposium*, 489-494.
Wu, J., and Juvkam-Wold, H. (1993), "Helical buckling of pipes in extended reach and horizontal wells - part 2: Frictional drag analysis", *J. of Energy Resources Technology*, **115**, 196-201.
Wu, J., and Juvkam-Wold, H.C. (1995), "Buckling and lockup of tubulars in inclined wellbores", *Transaction of the ASME*, **117**, 208-213.

Appendix: Transmission of the axial load

A.1 Approximation of the weight contact force

For drag analysis, only the normal projection of the weight must be taken into account. Therefore, this projection part, denoted N_1, depends on the angular position $\alpha(x)$ of the point along the duct wall and we have:

$$N_1(x) = \delta_i w_e \cos(\alpha(x)) = \delta_i w_e \beta(\alpha(x)) \tag{32}$$

Expressions for $\beta(\alpha(x))$ are now presented for the two buckling cases.

Sinusoidal post-buckling

The sinusoid increases along the duct until the wave reaches the middle of the duct. The relation between the highest amplitude, denoted α_0, and the applied load F_s must be explained. An assumption is made and concerns the variation of the amplitude which is supposed to be linear when the load increases from $F_{\sin}$ to F_{hel}. We have:

$$\alpha_0(F_{\sin}) = 0 \qquad \alpha_0(F_{\text{hel}}) = \frac{\pi}{2} \tag{33}$$

Therefore, the highest amplitude of the cable in the duct can be expressed as:

$$\alpha_0 = \frac{\pi}{2}\left(\frac{F_s - F_{\sin}}{F_{\text{hel}} - F_{\sin}}\right) = \frac{\pi}{2}\bar{F} \tag{34}$$

where $\bar{F}$ stands for $\dfrac{F_s - F_{\sin}}{F_{\text{hel}} - F_{\sin}}$.

As previously indicated, P_s denotes a half sinus pitch and a function ϕ, which is independent of the cable angular position, must be identified. Therefore, ϕ is given by:

$$\int_0^{P_s} \phi dx = \int_0^{P_s} \delta_i \beta(\alpha(x)) w_e dx \tag{35}$$

with

$$\beta(\alpha(x)) = \cos\left(\alpha_0 \sin\left(\frac{\pi x}{P_s}\right)\right)$$

Thus, we obtain:

$$\phi = 2\frac{w_e}{\pi\bar{F}} \sin\left(\frac{\pi\bar{F}}{2}\right) \tag{36}$$

Helical postbuckling

For the helical case, integration is performed on the pitch of the helix and we have $\beta(\alpha(x)) = 1$ on the lower part of the duct and $\beta(\alpha(x)) = -1$ on the upper part of the duct.

Therefore ϕ takes the obvious value:

$$\phi = 0 \tag{37}$$

A.2 The axial load

In order to obtain Eq. (27) for the sinus post-buckling case and Eq. (28) for the helical case, taking previous expressions for ϕ into account, the differential equation given in Eq. (21) must be integrated.

Sinusoidal post-buckling

The general differential equation of frictional drag takes the following form with $\delta_i = 1$ and $\eta = 8$:

$$\frac{dF}{dx} = \mu\left(\phi w_e + \frac{rF^2}{8EI}\right) \tag{38}$$

After some algebraic manipulations, the general solution is:

$$F_s(x) = \sqrt{\frac{8EI\phi}{r}}\tan\left\{\arctan\left(F\sqrt{\frac{r}{8EI\phi}}\right) - \mu x\sqrt{\frac{r\phi}{8EI}}\right\} \tag{39}$$

Helical post-bucking

In the same way, the differential equation is defined by:

$$\frac{dF}{dx} = \mu\frac{rF^2}{\eta EI} \tag{40}$$

The integration between F and $F(x)$ with respect to the coordinate x is performed and we obtain:

$$F_h(x) = \left(\frac{\mu r}{2EI}x + \frac{1}{F}\right)^{-1} \tag{41}$$

Nomenclature

α_0	: maximum angular perturbation (rad)
$\alpha(x)$	: angular perturbation (rad)
ΔV	: potential energy
ΔU	: bending energy
ΔW_{ext}	: external load work
ΔW_F	: applied compressive load work
ΔW_{weight}	: weight work
λN_2	: effect of the beam configuration in the contact force ($\text{N}\cdot\text{mm}^{-1}$)
μ	: friction coefficient
ϕ	: weight contact force approximation ($\text{N}\cdot\text{mm}^{-1}$)
EI	: beam bending modulus ($\text{N}\cdot\text{mm}^2$)
F_s	: axial compressive load (sinus configuration) (N)
F_{sin}	: sinusoidal critical load (N)
F_h	: axial compressive load (helical configuration) (N)
F_{hel}	: helical critical load (N)
L	: length of the beam (mm)
L_{hel}	: length of the beam in helical configuration (mm)
n	: number of half sinus or helical pitches

N : contact force ($N \cdot mm^{-1}$)
N_1 : weight participation in the contact force ($N \cdot mm^{-1}$)
P_h : constant pitch (helical configuration (mm)
P_{hel} : helical critical pitch (mm)
P_s : constrant half pitch (sinus configuration) (mm)
P_{sin} : half sinus critical pitch (mm)
r : clearance radius between the duct and the beam (mm)
w_e : beam weight ($N \cdot mm^{-1}$)
x : axial beam coordinate (mm)